Nanoscale

PAPER

View Article Online
View Journal

Cite this: DOI: 10.1039/c8nr06817h

Role of the Cu substrate in the growth of ultra-flat crack-free highly-crystalline single-layer graphene†

Benjamin Huet * and Jean-Pierre Raskin

Received 22nd August 2018,
Accepted 9th November 2018

DOI: 10.1039/c8nr06817h

rsc.li/nanoscale

Producing ultra-flat crack-free single-layer high-quality graphene over large areas has remained the key challenge to fully exploit graphene's potential into next-generation technological applications. In this regard, we show that epitaxial Cu(111) film represents the most promising catalyst for the chemical vapor deposition (CVD) of graphene with superior planarity and physical integrity. We first compare the most widely used Cu catalysts (foils, polycrystalline films and epitaxial films) in order to benchmark the roughness of the Cu surface which serves as a template for graphene growth. We then discuss the correlation between the formation of cracks and wrinkles in as-grown graphene and the surface morphology of these various Cu catalysts. In particular, Cu grain boundary grooves, inherently present in polycrystalline substrates, are found to contribute to the formation of cracks. Finally, we focused on tuning the CVD protocol in order to successfully grow highly crystalline graphene made of millimeter-size domains on every type of catalyst while mitigating Cu surface roughening. Putting into context the challenges and opportunities associated with the most widely used Cu catalysts provides valuable guidelines for high-throughput manufacturing of graphene suitable for emerging industrial applications.

1 Introduction

Due to its unique combination of excellent physical properties, graphene is envisioned to play a central role in a wide range of technological applications including high-frequency and flexible electronics,[1] solar cells,[2] organic light-emitting diodes,[3] and sensors.[4] Unfortunately, despite the relentless research efforts mobilized by the scientific community to improve graphene synthesis and processing, high performance graphene-based practical applications are not close to industrialization yet.[5,6] The chemical vapor deposition (CVD) of graphene on metals represents the most industrially viable production method as it yields continuous single- and few-layer graphene over extended surface areas at a relatively low cost.[7,8] CVD-grown graphene has already been successfully employed as top-gate for solar cells,[9] anti-corrosion and anti-scratch coatings,[10,11] and incorporated into basic flexible touch screens.[12] However, in order to fully exploit graphene's potential once integrated into micro- and nano-scale devices, the requirements are more stringent and four major aspects have to be considered: (i) a strict control over the number of layers, (ii) a high structural quality, (iii) the absence of cracks and wrinkles, and (iv) a planar geometry.

Due to its low carbon solubility (~7 ppm at 1050 °C) and its low catalytic activity, Cu remains the preferred catalytic material for growing graphene films with a thickness limited to a few layers.[13] Moreover, the weak Cu-graphene interaction is suitable for clean graphene transfer methods based on peeling rather than catalyst etching.[14] Over the last few years, improving the structural quality of the polycrystalline CVD-grown graphene has become key topic of CVD research. In addition to controlling the domain shape and orientation, a particular attention has been given to decreasing the density of graphene nuclei so that they can expand and become large single-crystalline domains before merging into a continuous graphene sheet.[15–18] Although different research groups reported the synthesis of graphene of millimeter- and even centimeter-scale graphene single crystals on Cu foils,[19–21] it has however been recently discovered that decreasing the nucleation site density also promotes the formation of undesired ad-layers.[22,23] This downside stems from the fact that, C based active species produced through methane adsorption on Cu foil backside, can diffuse through the Cu foil thickness and contribute to the growth of graphene on the Cu topside underneath the first growing graphene domain. On the other hand, crack, wrinkles and local stress are inherently present on as-grown graphene due to the high temperature required for the

Place du Levant, 3, 1348 Louvain-la-Neuve, Belgium.
E-mail: benjamin.huetb@gmail.com; Tel: +32 495444269

†Electronic supplementary information (ESI) available. See DOI: 10.1039/C8NR06817H

CVD process and thermal expansion mismatch between graphene and its substrate.[24,25] Finally, given that graphene growth follows the catalyst surface morphology, it is essential to employ a flat synthesis substrate in order to prevent the formation of additional wrinkles, cracks and local stress in the graphene sheet once transferred.[26,27]

Growing graphene on a thin Cu film pre-deposited on a flat and rigid substrate instead of commonly used Cu foils appears as a promising way to concomitantly tackle the four aforementioned aspects. Indeed, Cu film surface does not require any cumbersome polishing treatment to exhibit a relatively good planarity and offers a better control over the number of layers as the methane catalysis is constricted to the Cu film top surface. Up to now, graphene has been obtained using Cu films pre-deposited on mica cite,[28] SiO_2/Si,[29,30] fused quartz,[31,32] MgO,[33,34] spinel,[35] and sapphire[36,37] substrates. Unfortunately, the quasi-2D nature of the Cu film makes it more prone to degradation upon the high-temperature CVD process and hence makes it more difficult to produce large compact graphene single-crystalline domains.

In this work, we demonstrate that C-plane sapphire coated with a Cu film is an ideal platform to synthesize ultra-flat millimeter-size graphene domains free from cracks and possessing very shallow wrinkles. First, we put into context the relative surface roughness that can be obtained with the most widely employed Cu catalysts for the chemical vapor deposition of graphene including Cu foils, polycrystalline and epitaxial Cu films. This comparison thus provides a unified view of what can be expected in terms of graphene planarity when using Cu based catalytic substrates. By comparing the various catalytic platforms, we then show that the Cu surface morphology plays a critical role in the formation of wrinkles and cracks in as-grown graphene upon the cooling down of the CVD furnace. Particular emphasis is placed on epitaxial Cu films which yield superior graphene results in terms of planarity and integrity. Our experimental results suggest that exposing the Cu film to oxygen at high temperature prior to graphene growth promotes the formation of a low density of nucleation sites which is essential to produce large single-crystals of graphene but also negatively impacts the Cu surface morphology. Therefore, we focus on tailoring the CVD protocol conditions in order to produce large single-crystals of graphene while mitigating the Cu surface roughening. This work thereby enriches the general understanding of the challenges and opportunities regarding graphene production capabilities, which is of great importance to foster the emergence of graphene-based applications.

2 Results and discussion

Cu substrate surface roughness

To gain insight into the planarity of graphene that can be obtained using the most widely employed catalytic substrates, we systematically compared the surface roughness of commercial Cu foils and Cu films evaporated on both fused quartz and C-plane sapphire wafers. The Cu surface morphology measurements were studied by contact profilometry and atomic force microscopy (AFM). Fig. 1a outlines the Cu surface morphology obtained with the various substrates before and after different treatments. Cu foils typically exhibit a large surface roughness due to the presence of striations resulting from the cold-rolling manufacturing process (see Fig. 1c). Surface features and singularities can be attenuated during the CVD protocol when using a long-duration high-temperature Cu annealing step under ambient or superior pressure conditions prior to graphene growth.[38–40] The Cu evaporation and re-deposition process taking place when maintaining the Cu foil at 1050 °C for 6 hours helps smoothening the micro-scale Cu surface features but does not effectively remove the few microns-high ridges (see ESI section S1† for profilometer scans and images). Polishing the Cu foil prior to loading it into the CVD furnace has been demonstrated to efficiently suppress the cold-rolling striations.[41,42] Cu foil chemical-mechanical polishing (CMP) tends to leave submicrometer-scale scratches on the surface which rapidly vanish during the CVD protocol and lead to an improved surface morphology as shown in Fig. 1d. Cu foil surface morphology can also be improved using an electropolishing process but this technique requires a particular setup and is more complicated to implement.[43] Regardless of the polishing method and the roughness level achieved prior to the CVD process, the Cu foil surface morphology strongly declines upon the high temperature CVD thermal treatment. Cu grains and grain boundary grooves, which can reach a depth of a few micrometers, represent the main contributor to the high surface roughness measured on Cu foils.

Using Cu film deposited on flat and smooth substrates represents an interesting alternative to widely used Cu foils. When deposited at room temperature, Cu films are composed of crystallites with a lateral size in the 40–100 nm range and exhibit a surface roughness ranging from 1.3 to 3.8 nm (see ESI section S2†). Similarly to Cu foils, upon the CVD process, the microstructure of Cu films pre-deposited on amorphous SiO_2 (as it is the case for plain fused quartz or thermally oxidized silicon wafers) evolves to form micrometer-size Cu grains. The lateral size of Cu grains as well as the density and depths of Cu grain boundary grooves vary with the Cu film thickness as shown in Fig. 1e and f. Fig. 1a presents the surface roughness measured on Cu films with thicknesses of 800, 1600, 2400, and 4800 nm that have undergone a CVD process consisting of a 1 hour-long heating step and a 90 min-long high temperature graphene growth step (at 1050 °C) before cooling down to room temperature. 800 nm-thick Cu films feature Cu grains with a lateral size ranging from 2 to 60 μm while 4800 nm-thick films have grains that can reach a few hundreds of micrometers. Although extending the exposure to high temperature gives more time for Cu atoms self-diffusion and Cu grain boundary migration, and thus tends to promote the growth of Cu grains, their sizes rapidly stagnate after being kept at 1050 °C for a few minutes. Optical microscopy images in Fig. 1e and f thus represent a good

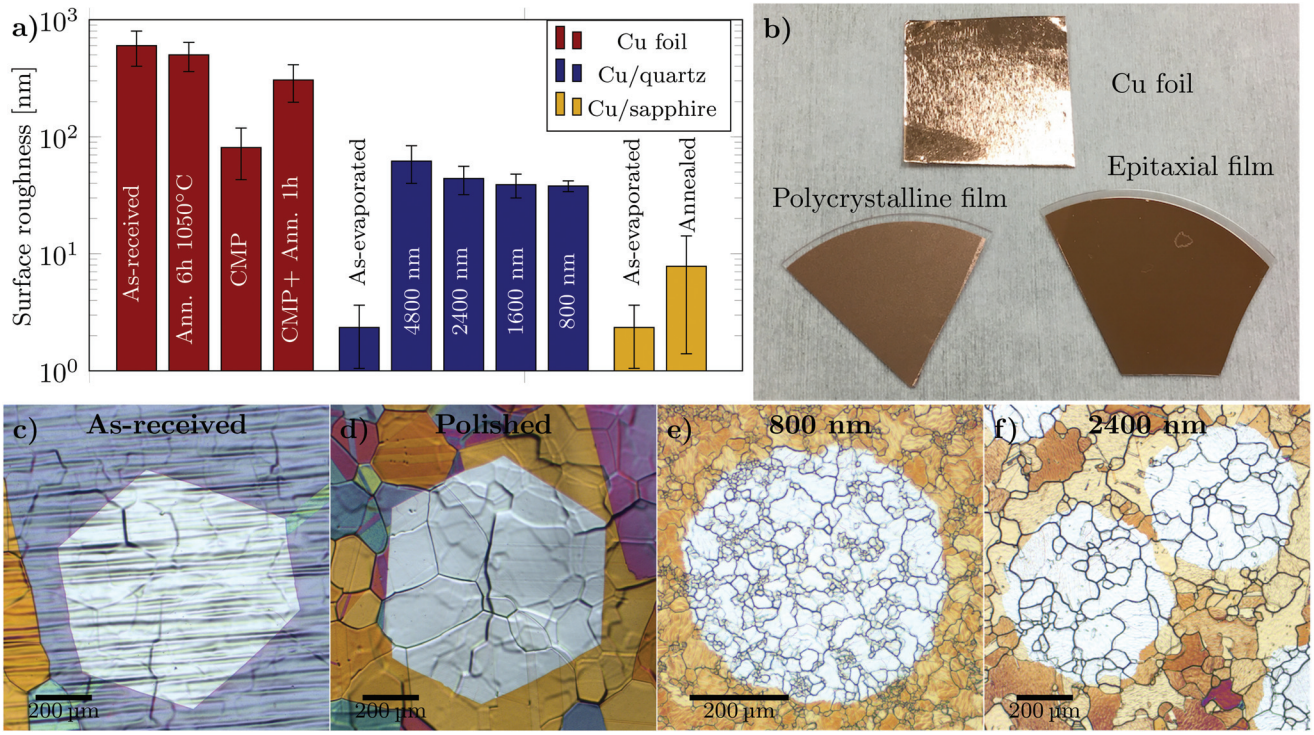

Fig. 1 (a) General overview of Cu surface (arithmetic average) roughness that can be obtained with Cu foils (red), Cu films on amorphous substrate (blue) and epitaxial films on C-plane sapphire. The error bars indicate the deviation of the roughness measured in at least 5 different locations on each sample. (b) Photograph of the most widely used Cu catalyst after the growth of graphene. (c–f) Optical microscope images of graphene domains (GDs) grown for 90 min at 1050 °C on (c) as-received and (d) polished Cu foils, and (e) 800 nm-thick and (f) 2400 nm-thick Cu films pre-deposited on a fused quartz wafer.

insight of the maximum lateral size of Cu grain that can be obtained for these thicknesses. Due to the small lattice mismatch between C-plane sapphire surface ($Al_2O_3(1000)$) and Cu(111), Cu films deposited on C-plane sapphire feature Cu grains that expand over several centimeters or even at the wafer-scale after being heated up to 1050 °C. Methods to improve the epitaxial relation between Cu and the underlying C-plane sapphire substrate have been discussed elsewhere.[44–46] The quasi absence of Cu grain boundary groove gives the Cu surface a superior morphology and a mirror-like visual appearance as shown in Fig. 1a and b, respectively. The epitaxial Cu surface roughness increase induced by the CVD process is further discussed in the next sections.

The surface roughness of the Cu substrate also impacts the physical integrity of graphene once transferred on a smooth and flat device-compatible substrate. Upon the transfer process, graphene is usually coupled with a mechanical support such as PMMA, thermal release tape or PDMS. This mechanical support acts as a rigid mold which maintains graphene's planar aspect after the Cu catalyst etching and the deposition on top of the final substrate. Once graphene is released from its mechanical support, it tends to conform to the underlying substrate. The difference between the actual graphene sheet surface area (which is closely related to the actual Cu surface area) and the projected surface area is directly correlated with the amount of wrinkles, cracks and strain that will be generated into the graphene sheet. This difference is non significant for epitaxial Cu film (≤0.005%), can reach a few percents for polycrystalline thin Cu films, and can even exceed 5% for Cu foils (see ESI section S1†). Owing to its low surface area difference, epitaxial Cu films therefore constitute top candidates as catalysts when attempting to make the most of graphene once embedded in practical devices.

As-grown graphene structural integrity

Cu substrate surface morphology does not only impact graphene planarity and its tendency to form wrinkles once transferred onto device-compatible substrates. In fact, it is found here that Cu surface morphology is one of the principal cause for the formation of wrinkles and cracks upon the final stage of the CVD process. These one-dimensional defects are known to negatively impact graphene's physical properties and must be avoided in order to achieve improved reliability, reproducibility and performance when fabricating graphene-based devices.[47,48] As shown in Fig. 2, various types of substrate result in markedly different graphene physical integrity, particularly with regards to the size, shape, density and location of wrinkles and cracks. Scanning electron microscopy (SEM) images have been acquired using in-lens (I-L) and regular Everhart–Thornley (E–T) secondary electron detectors in order to observe graphene's physical integrity (Fig. 2, first column) and the underlying Cu surface morphology (Fig. 2, second

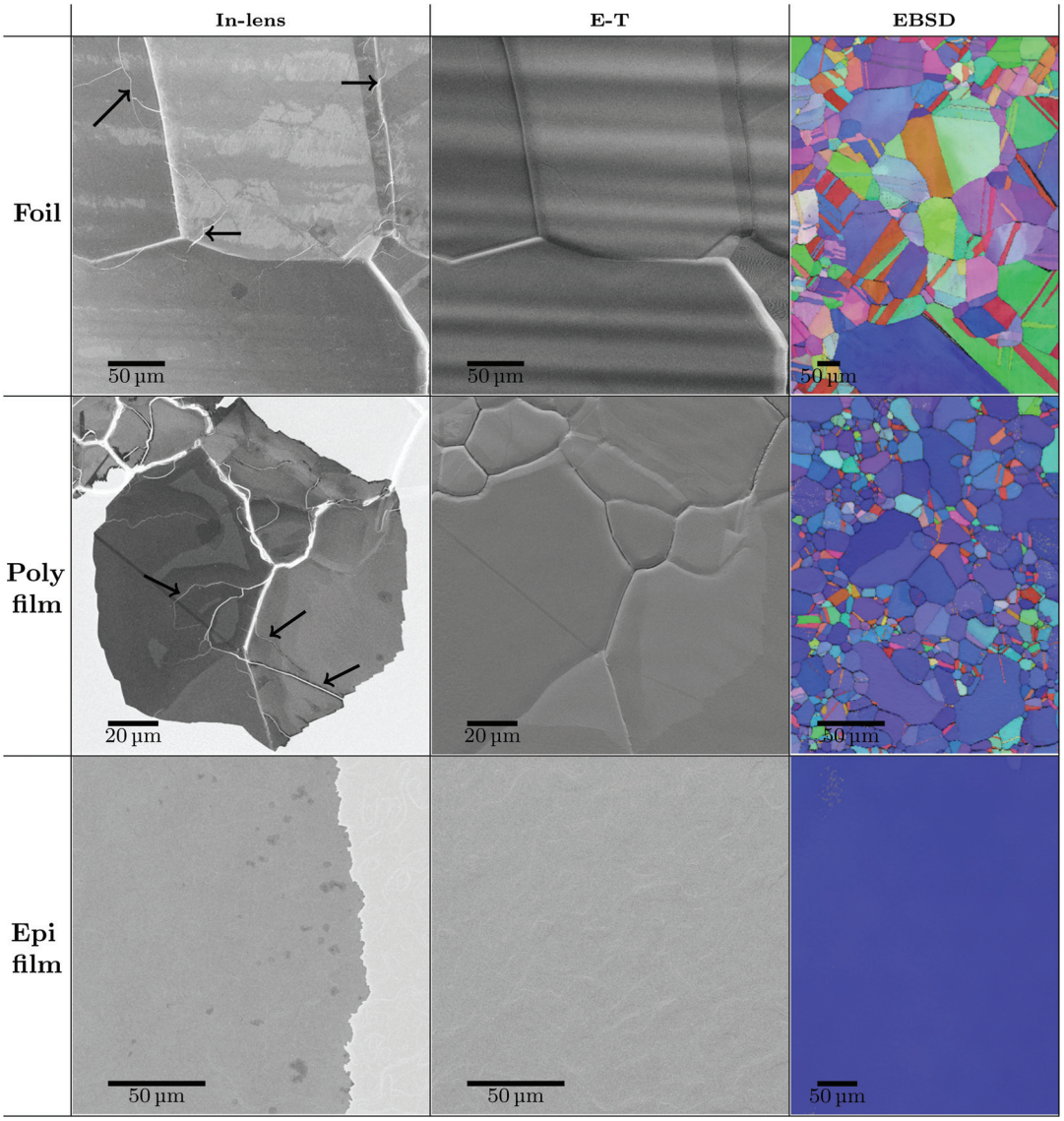

Fig. 2 Scanning electron microscopy images performed on Cu foils (top panel), polycrystalline Cu films (middle panel) and epitaxial Cu film (bottom panel). In-lens (first column) and regular E–T secondary electron (second column) SEM images taken in the same region to visualize graphene integrity and the underlying Cu surface morphology, respectively. Solid black arrows in in-lens images indicate the presence of cracks in graphene. Third column: Electron backscatter diffraction (EBSD) measurements taken on Cu foils, polycrystalline Cu films and epitaxial Cu film. Red, green and blue colors in the EBSD maps correspond to Cu(100), Cu(101), and Cu(111), respectively.

column), respectively. Electron backscattering diffraction (EBSD) measurements have also been performed to assess the Cu surface crystallographic orientation for each type of substrate as shown in the third column of Fig. 2.

Wrinkles typically form and build-up in the graphene sheet as it cools from the growth temperature down to room temperature (ΔT = 1050 °C–20 °C) due to compressive strain resulting from different thermal expansion coefficient (TEC) between graphene and the underlying substrate.[24] Although the scientific community agrees on the negative polarity of graphene's TEC (α_{gr}), its temperature dependency and room-temperature value are still under debate.[49–51] In the temperature range of interest, that is, in the 20–1050 °C range, it can be safely assumed that α_{gr} spans from −8 to -1×10^{-6} K^{-1}. In contrast, Cu has a positive TEC (α_{Cu}) which is about 16.7 × 10^{-6} K^{-1} at room temperature and can reach 19.8 × 10^{-6} K^{-1} at 900 °C.[52,53] On Cu foils, upon the furnace cooling down, the thermal coefficient mismatch gradually generates an in-plane compressive strain $\varepsilon \approx \Delta T(\alpha_{gr} - \alpha_{Cu})$ in graphene which can reach about 2%. Propagation of cracks in a certain direction is usually indicative of the presence of a tensile stress applied perpendicularly to the material.[54] While it is clear that wrinkles originate from the relaxation of the strong compressive strain in graphene, the fundamental mechanisms responsible for the formation of cracks during the CVD process are not well understood yet.[24,55]

The cracks observed in graphene grown on Cu foils can be sorted out in three categories depending on their location and the nature of their formation. The first category concerns the inevitable cracks that propagate across the Cu grain boundary grooves (white lines, Fig. 2, top panel). These cracks, characterized by the ~45° angle they form with the Cu grain boundaries, have been attributed to the shear stress present at the junction between adjacent Cu grains.[55] The presence of these kind of cracks can be mitigated by decreasing the density of Cu grain boundary grooves *via* an increase of the Cu grain size. The second category involves the cracks that develop into a rectilinear pattern within a given Cu grain and that cross graphene wrinkles perpendicularly (see ESI section S3† for additional SEM images).

Cracks from the same Cu grain are aligned in the same direction and those which spread over two adjacent Cu grains tend to change direction when crossing the Cu grain boundary. These are mostly found near the periphery of the Cu sample and are believed to be due to the deformation of the Cu foil upon cooling (see photograph in ESI section S3†). The edges of the Cu foil are more free to deform and tend to bend upward during the cooling down step of the CVD process (especially at $T \leq 400$ °C). This Cu foil macroscopic deformation can locally lead to an additional stress in the graphene film and results in cracks spreading over tens or hundreds of micrometers. The limited degree of freedom of the Cu foil central region, due to its closer contact with the support, more rarely contains these kinds of cracks. On the other hand, a prolonged exposure to high temperature tends to soften the Cu foil, improve its contact with the underlying quartz substrate used as a support, and cause the Cu foil to stick. If the Cu foil/support coupling is strong, the thermal dilatation of the support will contribute to the stress building up in graphene upon cooling and create cracks and wrinkles (see SEM images in ESI section S3†). It is therefore essential to maintain a proper balance between the exposure to high temperature and the ability of the foil to soften/bend which is mainly dictated by its thickness. The third kind of crack observed on graphene grown on Cu foils is caused by an indelicate handling of the Cu foil. They are readily recognizable as they spread over hundreds of micrometers, follow a clear pattern and are closely packed next to each other. Moreover, the presence of Cu grain boundaries has rather little or no effect on the pattern of these man-made cracks. The flexible nature of Cu foils makes graphene more prone to undergo extra deformation and stress, thus making it more challenging to study the formation of cracks and wrinkles.

In contrast, Cu films deposited on rigid substrates (including fused quartz, thermally oxidized Si and sapphire wafers) are more robust to bending and folding than Cu foils and can thus easily go through handling and graphene post-processing without any damage. Nevertheless, graphene grown on polycrystalline Cu films also contains cracks as shown in Fig. 2 (middle panel). In this case however, the vast majority of the cracks spread in a parallel fashion relatively to Cu grain boundary grooves and occasionally propagate over Cu grain in the shape of a lightning bolt. It can also be observed that graphene grown on Cu/quartz has rather shallow or no wrinkles. More SEM images of graphene grown on Cu film are available in ESI section S4.† When grown on epitaxial Cu films, graphene does not exhibit any cracks at all and has very shallow wrinkles that can only be seen using high magnification SEM imaging (see Fig. 2, bottom panel and ESI section S4†). The quasi-absence of wrinkles in graphene grown on epitaxial Cu films on sapphire has been recently observed and attributed to the relatively small in-plane thermal expansion of the Cu(111) thin film and relatively strong graphene/Cu(111) interfacial coupling compared to Cu(110) and Cu(100) orientations.[56,57] Our experimental results however suggest that the formation mechanisms of wrinkles and cracks are more complex than simply considering copper/graphene surface adhesion and thermal expansion mismatch.

On epitaxial and polycrystalline Cu films, the compressive strain in graphene is primarily governed by the thermal expansion of the C-plane sapphire and fused quartz wafers, respectively.[58] Indeed, upon cooling down, the 500 μm-thick quartz or sapphire substrates undergo thermal deformation which results in stress and strain in the thin Cu film deposited on its top.[59] C-plane sapphire has a thermal coefficient (parallel to the surface) varying from +6.6 to +9.0 × 10^{-6} K^{-1} when the temperature is increased from room temperature to 1000 °C.[60] On the other hand, in the 25–1050° C temperature range, fused quartz has a thermal coefficient varying between +4.0 and +6.0 × 10^{-6} K^{-1}.[61] By simply considering the TEC of the various substrates, graphene would be expected to undergo a relatively high level of deformation when grown on bulk Cu foils, an intermediate level of deformation when grown on Cu/sapphire and, a relatively low level of deformation when grown on Cu/quartz. On the other hand, graphene's ability for in-plane slipping and out-of-plane buckling depends on the crystallographic orientation of the underlying Cu surface as Cu(111), Cu(110) and Cu(100) have different compactness, surface energy, thermal dilatation coefficient and interaction with graphene.[56,62,63] It is thus expected that the graphene's structural integrity varies from one Cu grain to another, particularly in the case of Cu foils which is composed of a patchwork with a wide variety of Cu surface crystallographic orientations (see Fig. 2, third column). Finally, it is also very likely that there exists an interplay between the formation of wrinkles and the formation of cracks. Indeed, wrinkles can disrupt the pinning of graphene on the underlying surface, generate an inhomogeneous stress field, and eventually cause tensile stress localization leading to graphene cracking. These various considerations however fall short in explaining the shape, size and extent of wrinkles and cracks observed on the surface of the various substrates.

Our experimental observations suggest Cu surface morphology also plays a critical role in the formation of cracks and wrinkles. It is believed that the presence of Cu surface features such as Cu grain boundary grooves leads to a non uniform adhesion of graphene on the surface which thus induces strain/stress localization. Instead of having a uniform equi-

biaxial strain over the entire graphene sheet, strong localized strain is present in the vicinity of Cu grain boundaries that are characterized by steep step-terrace Cu surface structures on which graphene cannot maintain its pinning. Moreover, particularly in the case of the Cu/quartz stack, it is very likely that the Cu microstructure and surface morphology further evolve during the CVD process cooling step. Indeed, upon cooling and dilatation of the Cu/quartz stack, only a low stress can be sustained in the Cu film (see ESI section S5† for the residual stress calculation based on Stoney's formula). In order to accommodate the dilatation of the thick quartz substrate, the Cu film tends to creep.[64,65] This plastic deformation can take place through dislocation glide (temperature ≤100 °C) or Cu grain boundary diffusion (temperature ≥300 °C). The stress relaxation occurring in the Cu film in the vicinity of the Cu grain boundaries can thus be detrimental to graphene's physical integrity and provokes very localized cracks. Due to the presence of a relatively high density of cracks, the compressive stress present in graphene can be released and cannot accumulate over extended surface areas, thus leading to the quasi absence of wrinkles. In the case of epitaxial Cu films, the relatively strong graphene/Cu(111) coupling and then absence of Cu grain boundary grooves lead to a relatively uniform strain field in graphene and, therefore, no cracks and very shallow wrinkles. The presence of cracks with a ~45° angle in the Cu foil grain boundary grooves and spanning over a relatively short range is also indicative of a relatively low graphene adhesion/pinning on the Cu surface near the Cu grooves.

Interplay between domain density and surface roughness

Although epitaxial Cu films inherently have a more planar surface morphology compared with other types of catalyst, the surface roughness is however very sensitive to conditions employed during the CVD protocol. On the other hand, very specific CVD conditions have to be used in order to reduce the graphene nuclei density in the early stage of graphene formation, produce large single-crystalline graphene domains, and eventually obtain a low density of defect lines induced by the coalescence of misaligned domains.[66] Epitaxial Cu substrates, owing to their unique texture, have been found to produce well-aligned graphene domains whose orientation match with the Cu(111) hexagonal lattice, hence resulting in seamless graphene domain stitching.[35,67] Other research groups, however, reported that graphene does not systematically follow the underlying Cu(111) lattice and can exhibit other relative orientations including 3.4°,[35] 7°,[68] 9 ± 0.6°,[69] 30° (ref. 36) or, even random orientations.[70] On another note, it has also been reported that even well oriented adjacent domains could result in defect lines when merging together.[71] These defect lines can, for instance, serve as pathways for oxygen through the impermeable graphene sheet as it has been observed during our experiments (see ESI section S6†). Therefore, even on epitaxial Cu films, it is crucial to find approaches to avoid the formation of graphene grain boundaries.

Over the past few years, a series of papers demonstrated the interest of using pre-oxidized Cu substrates or CVD *in situ* Cu oxidation in order to reduce the nucleation site density.[20,21,72,73] Although the exact role of oxygen is still being debated among the scientific community, the most consistent explanation postulates that oxygen efficiently reduces the carbon content in the Cu catalyst prior to graphene growth.[22,74,75] The oxidative carbon removal employed for bulk Cu foils is however rather challenging to apply to thin Cu films that are more prone to undergo voiding, dewetting and hydrogen embrittlement.[32] It is found here that annealing the Cu substrate at high temperature in the presence of oxygen significantly reduces the nucleation site density of graphene but also tends to drastically deteriorate the Cu surface morphology.

To illustrate this finding, a systematic study has been conducted with both, as-deposited and *ex situ* oxidized Cu/sapphire substrates. Different CVD processes have been performed using exactly the same graphene growth step conditions (1050 °C, atmospheric pressure, hydrogen-to-methane ratio R = 440) but different pre-growth conditions as shown in Fig. 3a. These pre-growth conditions exclusively differ by the time and temperature at which hydrogen is introduced in the CVD furnace. The *ex situ* oxidized Cu film has been annealed on a hot plate in air at 200 °C for 2 min, creating a Cu oxide layer with a thickness of about 90 nm. On the other hand, the as-deposited Cu films gets gradually oxidized *in situ* as the CVD furnace heating proceeds due to trace amounts of oxygen present in the Ar flow. Introducing hydrogen into the CVD furnace plays a dual role: the oxygen traces brought to the catalyst by the argon flow is suppressed and the Cu oxide layer is reduced into its metallic form.

Fig. 3b shows that delaying the introduction of hydrogen results in the improvement of the graphene domain density by about three orders of magnitude. It can also be observed that the graphene domain density grown on as-deposited and on pre-oxidized Cu films is very similar. Optical images of graphene grown on *ex situ* oxidized epitaxial Cu film is available in ESI section S7.† ESI section S7† also provides bar charts of the graphene domain size obtained with the four CVD protocols displayed in Fig. 3a for both *in situ* and *ex situ* oxidized Cu films. This observation suggests that the key for reducing the nucleation site density lies into the temperature and exposure time in the presence of oxygen rather than the Cu oxide layer thickness/Cu oxidation extent. Introducing H_2 after 80 min enables the synthesis of graphene with a lateral size of about 600 μm for a graphene growth step duration (t_{gr}) of about 35 min (see Fig. 3f) while introducing it after 42 min leads to almost coalesced 10 μm-large domains after a t_{gr} of about 20 min (see Fig. 3c). Our Cu oxidation-assisted CVD approach can be used to routinely produce single crystalline graphene domains with a lateral size exceeding one millimeter on epitaxial Cu(111) thin films (after a growth duration $t_{gr} \geq 50$ min) as well as on polycrystalline Cu foils and films. To our knowledge, this result represents an improvement of about one order of magnitude compared with the literature which, up to now, reached a maximum lateral size of about 100 μm.[76] According to the trend plotted in Fig. 3b, maintaining the Cu film at high temperature for a longer duration in a hydrogen-free atmo-

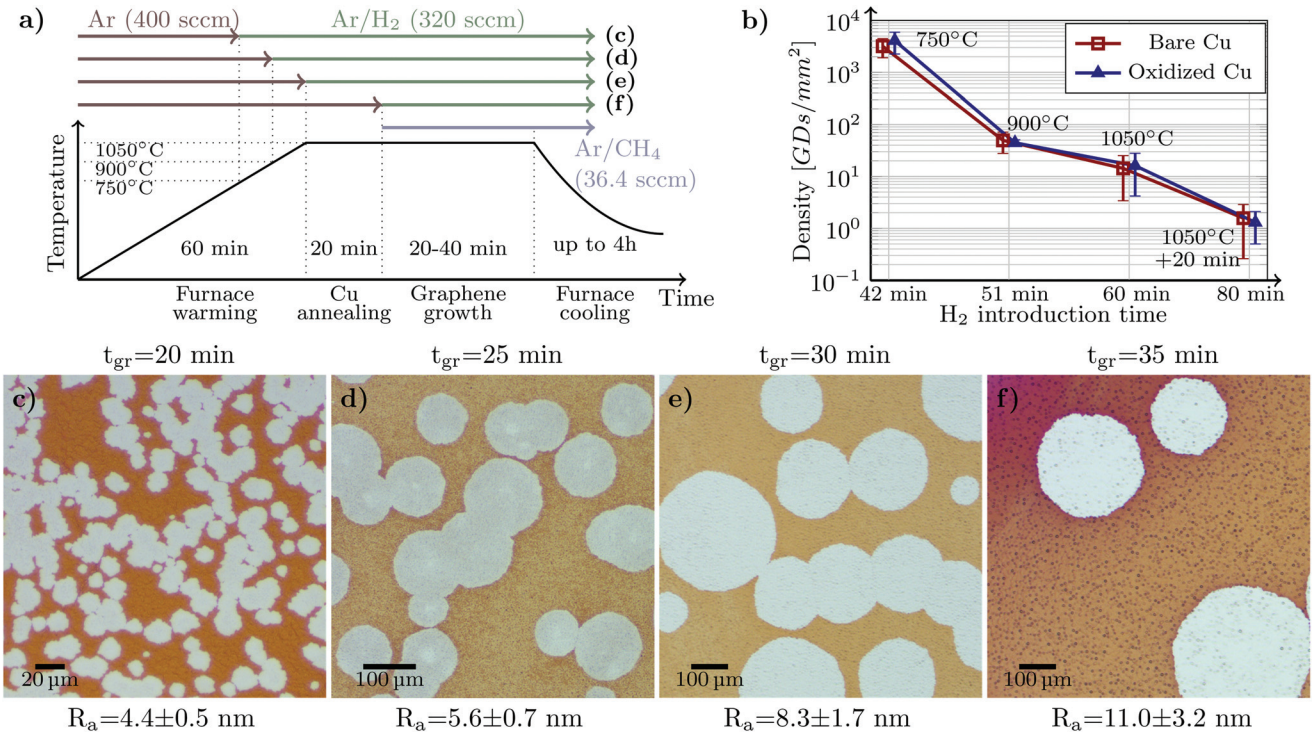

Fig. 3 (a) Temperature and gas flow rate profiles used for the graphene growth protocols. (b) Plot of the graphene domain density as a function of the time of hydrogen introduction in the CVD furnace for both as-deposited and oxidized Cu films. (c–f) Optical microscope images of graphene grown on epitaxial Cu film after a slight Cu oxidation to make graphene visible. Graphene growth results in (c), (d), (e), and (f) correspond to CVD processes involving the reduction of Cu surface oxide layer at 750 °C, 900 °C, 1050 °C, and after 20 min at 1050 °C, respectively. For each epitaxial Cu film samples, R_a values have been extracted from five 30 × 30 µm^2 AFM images acquired in different regions.

sphere would further decrease graphene domain density and eventually yield even larger graphene single crystals. Unfortunately, it is found that prolonged exposure to oxygen and excessive oxidation cause Cu surface roughening, voiding and even dewetting (see ESI section S8†).

It can also be observed in Fig. 3c–f that the Cu surface roughness varies with the hydrogen introduction delay. Fig. 4 compares the Cu surface morphology obtained when hydrogen is introduced at 750 °C and after 20 min at 1050 °C. An insight about the Cu surface roughness can be quickly obtained using a differential interference contrast (DIC) microscope (see Fig. 4a and b). Atomic force microscopy (AFM) measurements have been performed to get a more accurate information on the surface roughness. As shown in Fig. 4d, delaying the introduction of hydrogen tends to produce depressions in the Cu surface with a lateral size of about 10 micrometers and a depth exceeding 100 nanometers. These depressions are also visible using SEM microscopy as shown in ESI section S9.† Performing a CVD protocol similar to those shown in Fig. 3a but using exclusively a reducing atmosphere during the Cu heating and annealing steps results in a root mean squared roughness (RMS) around 1.7 nm (R_a = 1.35 nm) while the roughness estimated from the images in Fig. 4c and d are estimated to be 5.14 nm (R_a = 3.9 nm) and 18.6 nm (R_a = 14.2 nm), respectively. The high temperature annealing at high temperature in the presence of oxygen thus clearly plays a role in the strong surface morphology modification upon the CVD process. Intriguingly, the surface morphology of pre-oxidized and *in situ* oxidized obtained after the CVD process are very similar (see plot in ESI section S7†). This observation suggests that the thickness of the oxide layer does not really have an impact on the final Cu surface roughness. In the same vein, it is found that 80 min-long pre-growth *in situ* oxidation step does not create depressions in the Cu surface as it is observed after the graphene growth step (see ESI section S8† for images of the oxidized Cu surface). These depressions, which represent the major contribution to the Cu surface roughness, thus appear during the reduction of the Cu oxide layer upon the hydrogen arrival in the early stage of graphene formation. The surface morphology has been found to be drastically improved by decreasing the reduction rate of the Cu surface. The reduction rate can be decreased, for instance, by including a transient step in the CVD protocol consisting of diluted hydrogen flow (400 sccm of Ar + 10 sccm of Ar/H_2 for 10 min) prior to the graphene growth step (see detailed CVD protocol in ESI section S10†). Another approach to improve the Cu surface morphology consists of performing the Cu reduction step at a lower temperature but then requires a prolonged duration (*i.e.* about 40 min at 950 °C) in a non-reducing atmosphere in order to obtain a sufficiently low density of graphene domains that will be able to expand over more than 1 millimeter before coalescence. Such improved surface morphology

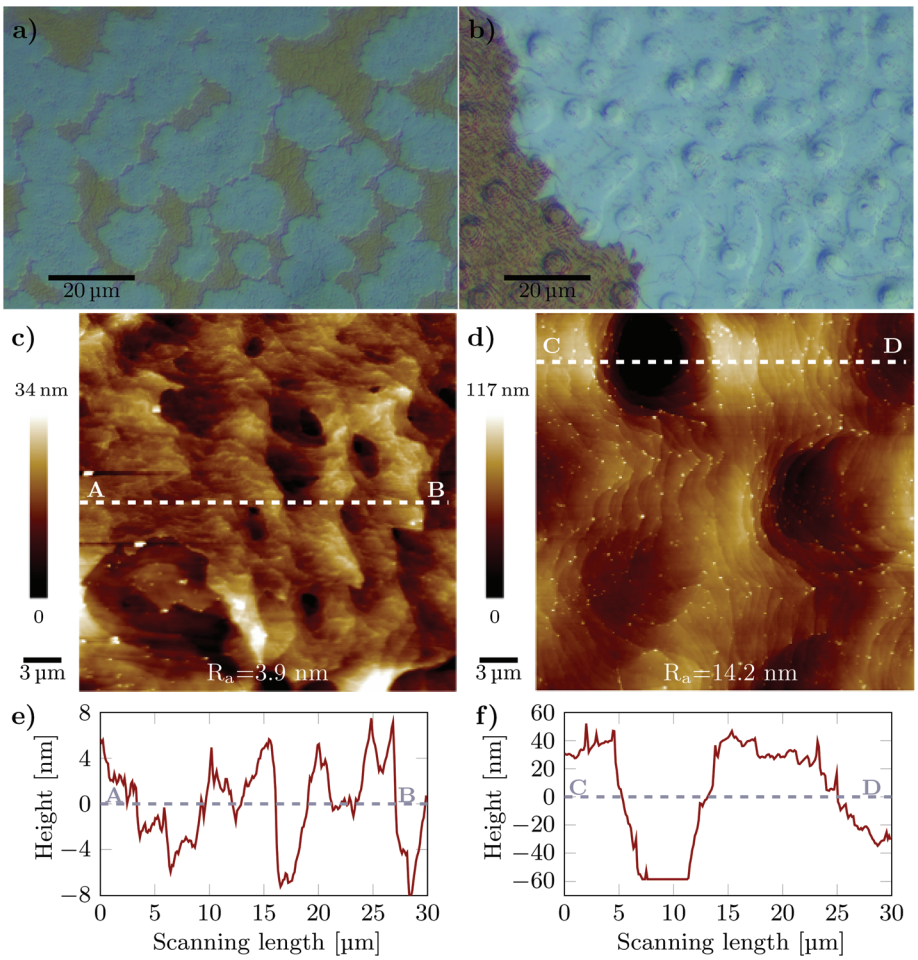

Fig. 4 (a–b) Differential interference contrast (DIC) microscopy images of graphene grown on epi Cu film when introducing hydrogen (a) at 750 °C and (b) after 20 min at 1050° C. (c) and (d) are atomic force microscopy images taken on graphene grown on epi Cu film that has been reduced at 750 °C and 1050 °C. (e) and (f) are AFM height profiles taken along the grey dashed line in (c) and (d), respectively.

is shown in Fig. 5a. At this stage, the Cu surface morphology is primarily governed by the surface step-bunching, that is, the formation of step and terraces on the Cu surface.[77] Consequently, the Cu surface roughness is sensitive to the Cu film thickness uniformity. Indeed, a variation of Cu film thickness impacts the height of the steps and the length of the terraces in a similar fashion as a miscut SiC wafer results in more steps and terraces upon the high temperature formation of epitaxial graphene.[78] When using a slow Cu surface reduction and a relatively conform Cu film (*i.e.* exhibiting a thickness variation across a 3 inch wafer inferior to 2%), the surface roughness R_a measured from 40 × 40 µm^2 AFM maps is in the 1.2–2.8 nm range.

Prior to this work, no research carefully investigated the influence of the Cu surface oxidation on the Cu surface roughness. This most likely stems from the fact that surface roughness is predominantly dictated by cold-rolling striations or Cu grain boundary grooves and the surface roughening effect of the Cu oxidation only represents a minor contributor to the surface roughness. In the case of epitaxial Cu films, the Cu oxidation-induced features represent the predominant contribution to the surface roughness.

Raman characterization

To assess the structural quality and the number of layers, we performed Raman spectroscopy directly on graphene as-grown on the epitaxial Cu film. In order to get a better insight about the uniformity of graphene deposition/growth, Raman mappings have been acquired on the entire graphene domain shown in Fig. 5a. The red (top) spectrum in Fig. 5b represents a typical Raman spectrum acquired directly on the catalyst as evidenced by the presence of the Cu background. The graphene-related G and 2D peaks are visible for Raman shift values of ~1585 cm^{-1} and ~2690 cm^{-1}, respectively. The very small or absent D peak normally located around 1350 cm^{-1} suggests very little or no structural defects in the graphene lattice.[79] The 2D peak is symmetrical and can be fitted by a single Lorentzian function which is a key characteristic of single-layer graphene or turbostractic bi- or tri-layer graphene.[80] Fig. 5b and c show that Raman spectra acquired on

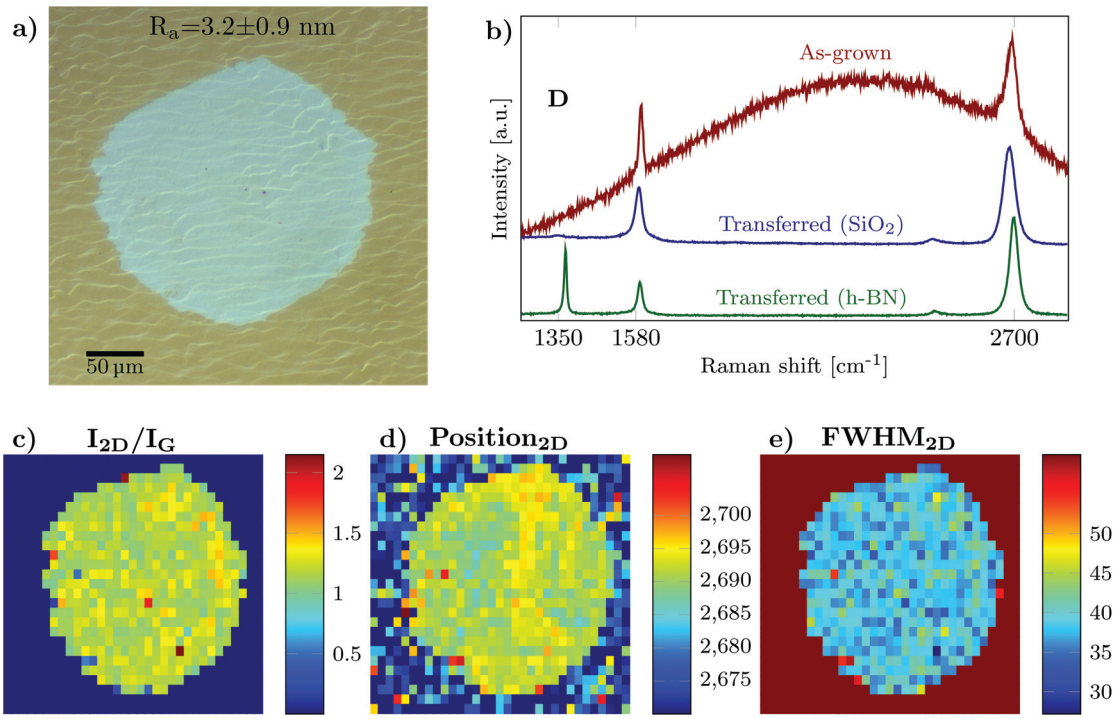

Fig. 5 (a) Differential interference contrast (DIC) microscopy images of graphene grown on epitaxial Cu film when introducing hydrogen at a slow rate. The surface roughness (R_a = 3.2 ± 0.9 nm or R_q = 4.05 ± 1.1 nm) has been extracted from five 40 × 40 µm^2 AFM maps acquired in different region of the wafer. (b) Raman spectra acquired directly on as-grown graphene on epitaxial Cu film and after transferring it on either a 300 nm thick thermal oxide or a h-BN flake. (c–e) Raman maps acquired directly on the graphene domain shown in (a). Maps in (c), (d) and (e) represent the I_{2D}/I_G peak intensity ratio, the 2D peak position and the 2D peak full width at half maximum.

as-grown graphene have an I_{2D}/I_G peak intensity ratio of about 1.3. Although pioneering works on Raman reported that single layer graphene typically features a I_{2D}/I_G of about 2, the intensity ratio strongly depends on the underlying substrate.[81,82] To verify the single layer nature of graphene produced on epitaxial Cu film, it has been transferred onto a Si/SiO_2 wafer with and without an exfoliated h-BN flake (purchased from Manchester Nanomaterial) pre-deposited on its top. Typical Raman spectra acquired on graphene/SiO_2 and on graphene/h-BN are plotted in Fig. 5b and exhibit a I_{2D}/I_G ratio of about 1.9 and 2.9, respectively. Owing to these I_{2D}/I_G values and a uniform optical contrast on 300 nm-thick SiO_2/Si substrate, it can be safely assumed that the as-produced graphene sheet is composed of one single layer (see ESI S9†). Fig. 5d and e display the position and the full width at half maximum (FWHM) of the 2D band which are comprised in the 2685–2695 cm^{-1} and in the 28–48 cm^{-1} ranges, respectively. These values are indicative of the presence of strain and nano-scale strain gradients over the graphene single-crystalline domain.[83] A more detailed Raman investigation is available in the ESI section S11.†

3. Conclusion

Our experimental investigation shows that the type of catalytic substrate is a key parameter to consider when manufacturing graphene and aiming to fabricate advanced graphene-based practical applications. This paper provides guidelines and solutions to address the major challenges related to the CVD production including controlling the planarity, suppressing cracks and wrinkles, and achieving a high structural quality. By comparing the Cu substrate surface roughness that can be obtained using the most widely employed catalysts (bare and polished Cu foils, polycrystalline Cu films and Cu(111) epitaxial film), we observed that as-produced graphene planarity can vary over 3 orders of magnitude. Graphene's physical integrity also markedly depends on the type of Cu substrate, particularly regarding the location, extent and shape of graphene cracks and wrinkles. Surface morphology features such as Cu grain boundaries are found to have a detrimental impact on the planarity of graphene and almost invariably cause the graphene film to crack. Our comparative study thus deepens our understanding of the mechanical and interfacial behavior of graphene on its synthesis substrate. Oxidative carbon removal is a facile and efficient approach to produce highly crystalline graphene on every types of Cu substrate but has been found to impair Cu surface morphology. This roughening effect has been found to be mitigated by slowing down the reduction of Cu oxide into Cu prior to graphene growth. The selection of the Cu substrate employed for the CVD process has substantial consequences on the planarity and physical integrity of graphene and should therefore be carefully considered in the

realization and interpretation of a broad range of existing and future research.

4. Experimental methods

The CVD protocols were performed in a horizontal hot-wall CVD furnace (1.2 meter-long, 10 cm inner diameter, purchased to MTI corporation) under atmospheric pressure. Gas feedstock were supplied by Praxair: Ar (99.999%), Ar/CH_4 (2000 ppm) and Ar/H_2 (10%). Cu foils (50 μm-thick, 99.9% purity) were purchased to Advent Research Materials (UK). Fused quartz (JGS2, $R_a \leq 1.2$ nm) and C-plane sapphire (single-side surface polished Epi ready) wafers were purchased to Prime Wafers (NL). Cu films were deposited by electron beam evaporation at room temperature (4 Å s^{-1}, pressure $\sim 2 \times 10^{-7}$ mbar) using 99.999% pure Cu pellets from Kurt J. Lesker. The samples were characterized using Raman spectroscopy (LabRAM HR by Horiba, excitation energy: 2.41 eV/514 nm, spot size: ~1 μm), SEM (Zeiss Gemini Ultra-55, EHT: 3 kV, working distance ≤3 mm), AFM (Dimension Icon Instrument by Bruker, Peak Force tapping mode in air, linear scanning rate: 0.5–1 Hz, set point: 400–1000 mV), and EBSD (electron energy: 15–20 kV, step size: 0.75 μm). Cu foils were polished using the Struers protocol with a mechanical polishing (MD-Mol, 20 min) and an oxide polishing (MD-Chem, 2 min). Graphene has been transferred onto a 300 nm-thick Si/SiO_2 substrate using the wet PMMA-assisted method. A more detailed description of the transfer process is provided in ESI section S11.†

Conflicts of interest

There are no conflicts to declare.

Acknowledgements

We gratefully thank Pascal Jacques and the IMMC institute for the EBSD measurements. We acknowledge the financial support from the Fonds Nationaux de la Recherche Scientifique (FNRS-Belgium) and the Fonds pour la Formation à la Recherche dans l'Industrie et dans l'Agriculture (FRIA-Belgium). In addition, we gratefully acknowledge the Wallonia Infrastructure for Nano FABrication (WINFAB) for the equipments and the Wallonia ELectronics and COMmunications measurements (WELCOME) platform for the micro Raman system.

References

1 W. Wei, E. Pallecchi, S. Haque, S. Borini, V. Avramovic, A. Centeno, Z. Amaia and H. Happy, *Nanoscale*, 2016, **8**, 14097–14103.
2 Y. Song, S. Chang, S. Gradecak and J. Kong, *Adv. Energy Mater.*, 2016, **6**, 1600847.
3 T.-L. Wu, C.-H. Yeh, W.-T. Hsiao, P.-Y. Huang, M.-J. Huang, Y.-H. Chiang, C.-H. Cheng, R.-S. Liu and P.-W. Chiu, *ACS Appl. Mater. Interfaces*, 2017, **9**, 14998–15004.
4 O. Moldovan, B. Iñiguez, M. J. Deen and L. F. Marsal, *IET Circ. Devices Syst.*, 2015, **9**, 446–453.
5 K. S. Novoselov, V. I. Falko, L. Colombo, P. R. Gellert, M. G. Schwab and K. Kim, *Nature*, 2012, **490**, 192.
6 A. Zurutuza and C. Marinelli, *Nat. Nanotechnol.*, 2014, **9**, 730–734.
7 X. Li, W. Cai, J. An, S. Kim, J. Nah, D. Yang, R. Piner, A. Velamakanni, I. Jung, E. Tutuc, S. K. Banerjee, L. Colombo and R. S. Ruoff, *Science*, 2009, **324**, 1312–1314.
8 S. Hofmann, P. Braeuninger-Weimer and R. S. Weatherup, *J. Phys. Chem. Lett.*, 2015, **6**, 2714–2721.
9 F. Lang, M. A. Gluba, S. Albrecht, J. Rappich, L. Korte, B. Rech and N. H. Nickel, *J. Phys. Chem. Lett.*, 2015, **6**, 2745–2750.
10 R. S. Weatherup, L. Darsié, A. Cabrero-Vilatela, S. Caneva, R. Blume, J. Robertson, R. Schloegl and S. Hofmann, *J. Am. Chem. Soc.*, 2015, **137**, 14358–14366.
11 M. Hammad, J.-J. Adjizian, C.-H. Sacré, B. Huet, J.-C. Charlier, J.-P. Raskin and T. Pardoen, *Carbon*, 2017, **122**, 446–450.
12 S. Bae, H. Kim, Y. Lee, X. Xu, J.-S. Park, Y. Zheng, J. Balakrishnan, T. Lei, H. Ri Kim, Y. I. Song, Y.-J. Kim, K. S. Kim, B. Ozyilmaz, J.-H. Ahn, B. H. Hong and S. Iijima, *Nat. Nanotechnol.*, 2010, **5**, 574–578.
13 G. Lopez and E. Mittemeijer, *Scr. Mater.*, 2004, **51**, 1–5.
14 L. Banszerus, M. Schmitz, S. Engels, J. Dauber, M. Oellers, F. Haupt, K. Watanabe, T. Taniguchi, B. Beschoten and C. Stampfer, *Sci. Adv.*, 2015, **1**, 6.
15 X. Li, C. W. Magnuson, A. Venugopal, J. An, J. W. Suk, B. Han, M. Borysiak, W. Cai, A. Velamakanni, Y. Zhu, L. Fu, E. M. Vogel, E. Voelkl, L. Colombo and R. S. Ruoff, *Nano Lett.*, 2010, **10**, 4328–4334.
16 A. T. Murdock, A. Koos, T. B. Britton, L. Houben, T. Batten, T. Zhang, A. J. Wilkinson, R. E. Dunin-Borkowski, C. E. Lekka and N. Grobert, *ACS Nano*, 2013, **7**, 1351–1359.
17 D. Ding, P. Solis-Fernandez, H. Hibino and H. Ago, *ACS Nano*, 2016, **10**, 11196–11204.
18 V. Miseikis, F. Bianco, J. David, M. Gemmi, V. Pellegrini, M. Romagnoli and C. Coletti, *2D Mater.*, 2017, **4**, 021004.
19 S. Chen, H. Ji, H. Chou, Q. Li, H. Li, J. W. Suk, R. Piner, L. Liao, W. Cai and R. S. Ruoff, *Adv. Mater.*, 2013, **25**, 2062–2065.
20 Y. Hao, M. S. Bharathi, L. Wang, Y. Liu, H. Chen, S. Nie, X. Wang, H. Chou, C. Tan, B. Fallahazad, H. Ramanarayan, C. W. Magnuson, E. Tutuc, B. I. Yakobson, K. F. McCarty, Y.-W. Zhang, P. Kim, J. Hone, L. Colombo and R. S. Ruoff, *Science*, 2013, **342**, 720–723.
21 J. Li, X.-Y. Wang, X.-R. Liu, Z. Jin, D. Wang and L.-J. Wan, *J. Mater. Chem. C*, 2015, **3**, 3530–3535.
22 B. Huet and J.-P. Raskin, *Carbon*, 2018, **129**, 270–280.

23 I. H. Abidi, Y. Liu, J. Pan, A. Tyagi, M. Zhuang, Q. Zhang, A. A. Cagang, L.-T. Weng, P. Sheng, W. A. Goddard and Z. Luo, *Adv. Funct. Mater.*, 2017, **27**, 1700121.
24 S. Deng and V. Berry, *Mater. Today*, 2016, **19**, 197–212.
25 W. Wang, S. Yang and A. Wang, *Sci. Rep.*, 2017, **7**, 8244.
26 N. Liu, Z. Pan, L. Fu, C. Zhang, B. Dai and Z. Liu, *Nano Res.*, 2011, **4**, 996–1004.
27 V. E. Calado, G. F. Schneider, A. M. M. G. Theulings, C. Dekker and L. M. K. Vandersypen, *Appl. Phys. Lett.*, 2012, **101**, 103116.
28 J. L. Qi, K. Nagashio, T. Nishimura and A. Toriumi, *Nanotechnology*, 2014, **25**, 185602.
29 C.-Y. Su, A.-Y. Lu, C.-Y. Wu, Y.-T. Li, K.-K. Liu, W. Zhang, S.-Y. Lin, Z.-Y. Juang, Y.-L. Zhong, F.-R. Chen and L.-J. Li, *Nano Lett.*, 2011, **11**, 3612–3616.
30 C. Howsare, X. Weng, V. Bojan, D. Snyder and J. Robinson, *Nanotechnology*, 2012, **23**, 13.
31 A. Ismach, C. Druzgalski, S. Penwell, A. Schwartzberg, M. Zheng, A. Javey, J. Bokor and Y. Zhang, *Nano Lett.*, 2010, **10**, 1542–1548.
32 B. Huet and J.-P. Raskin, *Chem. Mater.*, 2017, **29**, 3431–3440.
33 Y. Ogawa, B. Hu, C. M. Orofeo, M. Tsuji, K.-i. Ikeda, S. Mizuno, H. Hibino and H. Ago, *J. Phys. Chem. Lett.*, 2012, **3**, 219–226.
34 R. M. Jacobberger and M. S. Arnold, *Chem. Mater.*, 2013, **25**, 871–877.
35 H. Ago, Y. Ohta, H. Hibino, D. Yoshimura, R. Takizawa, Y. Uchida, M. Tsuji, T. Okajima, H. Mitani and S. Mizuno, *Chem. Mater.*, 2015, **27**, 5377–5385.
36 B. Hu, H. Ago, Y. Ito, K. Kawahara, M. Tsuji, E. Magome, K. Sumitani, N. Mizuta, K. ichi Ikeda and S. Mizuno, *Carbon*, 2012, **50**, 57–65.
37 L. F. Lampert, R. Caudillo, T. Lindner and J. Jiao, *J. Phys. Chem. C*, 2016, **120**, 26498–26507.
38 Z. Yan, J. Lin, Z. Peng, Z. Sun, Y. Zhu, L. Li, C. Xiang, E. L. Samuel, C. Kittrell and J. M. Tour, *ACS Nano*, 2012, **6**, 9110–9117.
39 H. Wang, G. Wang, P. Bao, S. Yang, W. Zhu, X. Xie and W.-J. Zhang, *J. Am. Chem. Soc.*, 2012, **134**, 3627–3630.
40 S. Suzuki, T. Nagamori, Y. Matsuoka and M. Yoshimura, *Jpn. J. Appl. Phys.*, 2014, **53**, 095101.
41 G. H. Han, F. Gunes, J. J. Bae, E. S. Kim, S. J. Chae, H.-J. Shin, J.-Y. Choi, D. Pribat and Y. H. Lee, *Nano Lett.*, 2011, **11**, 4144–4148.
42 P. Braeuninger-Weimer, B. Brennan, A. J. Pollard and S. Hofmann, *Chem. Mater.*, 2016, **28**, 8905–8915.
43 M. H. Griep, E. Sandoz-Rosado, T. M. Tumlin and E. Wetzel, *Nano Lett.*, 2016, **16**, 1657–1662.
44 S. Curiotto, H. Chien, H. Meltzman, P. Wynblatt, G. S. Rohrer, W. D. Kaplan and D. Chatain, *Acta Mater.*, 2011, **59**, 5320–5331.
45 D. L. Miller, M. W. Keller, J. M. Shaw, K. P. Rice, R. R. Keller and K. M. Diederichsen, *AIP Adv.*, 2013, **3**, 082105.
46 K. Verguts, B. Vermeulen, N. Vrancken, K. Schouteden, C. Van Haesendonck, C. Huyghebaert, M. Heyns, S. De Gendt and S. Brems, *J. Phys. Chem. C*, 2016, **120**, 297–304.
47 C. S. Jin, G. Fethullah, K. K. Kang, K. E. Sung, H. G. Hee, K. S. Min, S. Hyeon-Jin, Y. Seon-Mi, C. Jae-Young, P. M. Ho, Y. C. Woong, P. Didier and L. Y. Hee, *Adv. Mater.*, 2009, **21**, 2328–2333.
48 W. Zhu, T. Low, V. Perebeinos, A. A. Bol, Y. Zhu, H. Yan, J. Tersoff and P. Avouris, *Nano Lett.*, 2012, **12**, 3431–3436.
49 N. Mounet and N. Marzari, *Phys. Rev. B: Condens. Matter Mater. Phys.*, 2005, **71**, 205214.
50 W. Bao, F. Miao, Z. Chen, H. Zhang, W. Jang, C. Dames and C. N. Lau, *Nat. Nanotechnol.*, 2009, **4**, 562–566.
51 D. Yoon, Y.-W. Son and H. Cheong, *Nano Lett.*, 2011, **11**, 3227–3231.
52 F. R. Kroeger and C. A. Swenson, *J. Appl. Phys.*, 1977, **48**, 853–864.
53 P. Hidnert and G. Dickson, *J. Res. Natl. Bur. Stand.*, 1943, **31**, 77.
54 S. R. Na, X. Wang, R. D. Piner, R. Huang, C. G. Willson and K. M. Liechti, *ACS Nano*, 2016, **10**, 9616–9625.
55 Y. Fan, K. He, H. Tan, S. Speller and J. H. Warner, *Chem. Mater.*, 2014, **26**, 4984–4991.
56 B. Deng, Z. Pang, S. Chen, X. Li, C. Meng, J. Li, M. Liu, J. Wu, Y. Qi, W. Dang, H. Yang, Y. Zhang, J. Zhang, N. Kang, H. Xu, Q. Fu, X. Qiu, P. Gao, Y. Wei, Z. Liu and H. Peng, *ACS Nano*, 2017, **11**, 12337–12345.
57 L. Bao-Wen, L. Da, Z. Liyan, Z. Xu, J. Sunghwan, H. Ming, D. Feng and R. S. Ruoff, *Adv. Mater.*, 2018, **30**, 1706504.
58 G. G. Stoney, *Proc. R. Soc. London, Ser. A*, 1909, **82**, 172–175.
59 K. Barmak and K. Coffey, *Metallic films for electronic, optical and Magnetic applications*, Woodhead, 2014.
60 E. R. Dobrovinskaya, L. A. Lytvynov and V. Pishchik, *Sapphire: Material, Manufacturing, Applications*, Springer, 2009.
61 J. Oishi and T. Kimura, *Metrologia*, 1969, **5**, 50.
62 O. Frank, J. Vejpravova, V. Holy, L. Kavan and M. Kalbac, *Carbon*, 2014, **68**, 440–451.
63 S. D. Costa, J. E. Weis, O. Frank and M. Kalbac, *Carbon*, 2015, **93**, 793–799.
64 M. Thouless, J. Gupta and J. Harper, *J. Mater. Res.*, 1993, **8**, 1845–1852.
65 M. J. Kobrinsky, C. V. Thompson and M. E. Gross, *J. Appl. Phys.*, 2001, **89**, 91–98.
66 O. V. Yazyev and Y. P. Chen, *Nat. Nanotechnol.*, 2014, **9**, 755–767.
67 V. L. Nguyen, B. G. Shin, D. L. Duong, S. T. Kim, D. Perello, Y. J. Lim, Q. H. Yuan, F. Ding, H. Y. Jeong, H. S. Shin, S. M. Lee, S. H. Chae, Q. A. Vu, S. H. Lee and Y. H. Lee, *Adv. Mater.*, 2014, **27**, 1376–1382.
68 L. Gao, J. R. Guest and N. P. Guisinger, *Nano Lett.*, 2010, **10**, 3512–3516.
69 C. Jeon, H.-N. Hwang, W.-G. Lee, Y. G. Jung, K. S. Kim, C.-Y. Park and C.-C. Hwang, *Nanoscale*, 2013, **5**, 8210–8214.
70 S. Gottardi, K. Müller, L. Bignardi, J. C. Moreno-López, T. A. Pham, O. Ivashenko, M. Yablonskikh, A. Barinov, J. Björk, P. Rudolf and M. Stöhr, *Nano Lett.*, 2015, **15**, 917–922.

71 L. Vicarelli, S. J. Heerema, C. Dekker and H. W. Zandbergen, *ACS Nano*, 2015, **9**, 3428–3435.
72 L. Gan and Z. Luo, *ACS Nano*, 2013, **7**, 9480–9488.
73 J. Pang, A. Bachmatiuk, L. Fu, C. Yan, M. Zeng, J. Wang, B. Trzebicka, T. Gemming, J. Eckert and M. H. Rummeli, *J. Phys. Chem. C*, 2015, **119**, 13363–13368.
74 J. Kraus, M. Böbel and S. Günther, *Carbon*, 2016, **96**, 153–165.
75 B. Liu, N. Xuan, K. Ba, X. Miao, M. Ji and Z. Sun, *Carbon*, 2017, **119**, 350–354.
76 H. Ago, K. Kawahara, Y. Ogawa, S. Tanoue, M. A. Bissett, M. Tsuji, H. Sakaguchi, R. J. Koch, F. Fromm, T. Seyller, K. Komatsu and K. Tsukagoshi, *Appl. Phys. Express*, 2013, **6**, 075101.
77 D. Yi, D. Luo, Z.-J. Wang, J. Dong, X. Zhang, M.-G. Willinger, R. S. Ruoff and F. Ding, *Phys. Rev. Lett.*, 2018, **120**, 246101.
78 J. A. Robinson, K. A. Trumbull, M. LaBella, R. Cavalero, M. J. Hollander, M. Zhu, M. T. Wetherington, M. Fanton and D. W. Snyder, *Appl. Phys. Lett.*, 2011, **98**, 222109.
79 A. C. Ferrari and D. M. Basko, *Nat. Nanotechnol.*, 2013, **8**, 235–246.
80 D. R. Lenski and M. S. Fuhrer, *J. Appl. Phys.*, 2011, **110**, 013720.
81 Y. y. Wang, Z. h. Ni, T. Yu, Z. X. Shen, H. m. Wang, Y. h. Wu, W. Chen and A. T. Shen Wee, *J. Phys. Chem. C*, 2008, **112**, 10637–10640.
82 L. Malard, M. Pimenta, G. Dresselhaus and M. Dresselhaus, *Phys. Rep.*, 2009, **473**, 51–87.
83 C. Neumann, S. Reichardt, P. Venezuela, M. Drögeler, L. Banszerus, M. Schmitz, K. Watanabe, T. Taniguchi, F. Mauri, B. Beschoten, S. V. Rotkin and C. Stampfer, *Nat. Commun.*, 2015, **6**, 8429.